Effect of the Organoclay Preparation on the Extent of Intercalation/Exfoliation and Barrier Properties of Polyethylene/PA6/Montmorillonite Nanocomposites

Eleonora Erdmann,[1] Delicia Acosta,[1] Victor J. R. R. Pita,[2] Fernanda E. Monasterio,[1] María C. Carrera,[1] Marcos L. Dias,[2] Hugo A. Destéfanis[1]

[1]*Instituto de Investigaciones para la Industria Química - INIQUI-CONICET-ANPCyT, Consejo de Investigaciones - CIUNSa, Facultad de Ingeniería - UNSa, Buenos Aires 177-4400, Salta, Argentina*
[2]*Instituto de Macromoléculas Professora Eloisa Mano - IMA, Universidad Federal do Rio de Janeiro, C.P., Río do Janiero 68525, 21945-970, Brazil*

Received 3 February 2009; accepted 1 April 2010
DOI 10.1002/app.32560
Published online 22 June 2010 in Wiley InterScience (www.interscience.wiley.com).

ABSTRACT: Nanocomposites of HDPE matrix and 3 wt % organoclay/PA6 discontinuous phase were prepared in a mixer chamber. These nanocomposites of organoclay, PA6, and HDPE were characterized by X-ray diffraction, scanning electron and transmission electron microscopy (SEM and TEM). Barrier properties were determined by cyclohexane pervaporation and solubility. The results show that the degree of exfoliation and/or intercalation and the barrier properties depend on a combination of the proper chemical treatment and optimized processing in these polyethylene-organoclays nanocomposites. © 2010 Wiley Periodicals, Inc. J Appl Polym Sci 118: 2467–2474, 2010

Key words: nanocomposites; barrier properties; organoclay; pervaporation; nylon6; high-density polyethylene

INTRODUCTION

High Density Polyethylene (HDPE) is probably the most used material for fabrication of containers for packing of hydrocarbon solvents, because it is recognized as chemical resistant, lightweight, and low-cost material. Although polyethylene has good barrier properties to polar solvents, it has poor barrier properties to nonpolar solvents, which make it a potential actor for environmental pollution, safety, and health problems.

Many techniques have been applied to solve this problem, such as surface treatment by fluorination or sulfonation, multilayer coextrusion with polyamide-6 (PA6), laminar blend blow molding with PA6, or polymer blend composites with PA6. Although these techniques have been successfully applied, polymer nanocomposite technology arises as an interesting alternative, because by employing minimal levels of fillers (<10 wt %), nanofillers can enhance mechanical, thermal, and barrier properties, particularly using exfoliated clays.[1–3] In spite of modified clays are usually miscible with polar polymers as polyamide, it does not disperse well in nonpolar polymer such as polypropylene and polyethylene.

Correspondence to: E. Erdmann (eleonora@unsa.edu.ar).

Journal of Applied Polymer Science, Vol. 118, 2467–2474 (2010)

To prepare exfoliated or intercalated polymer nanocomposites, organically modified clays can be incorporated in the polymer matrix from different ways. One important industrial strategy has been the preparation of polymer/organically modified clay nanocomposites by using extrusion, usually called melt intercalation process. Another way is the *in situ* intercalative polymerization.[4–6]

In general, barrier properties of polymer nanocomposites are highly dependent on the resulting morphology. However, it is very important to point out that in the case of PE/PA6 blends the barrier properties of PA6 itself are key factors in determining the barrier properties of the blends.[7–11]

The aim of this work was to show that the degree of clay delamination and dispersion depends on a combination of the proper chemical treatment and optimized processing and how this affects the barrier properties of HDPE/PA6/clay. Polymer/clay nanocomposites were prepared by two techniques: one of them using melt intercalation process and the other a combination of *in situ* polymerization and melt intercalation process. Barrier properties of HDPE/PA6/clay nanocomposites were studied by cyclohexane pervaporation. The influence of exfoliation and/or intercalation of clay platelets on solvent barrier were examined. In addition, the morphologies of HDPE/PA6/modified clay nanocomposites were studied by X-ray diffraction (XRD), scanning electron and transmission electron microscopy (SEM and TEM).

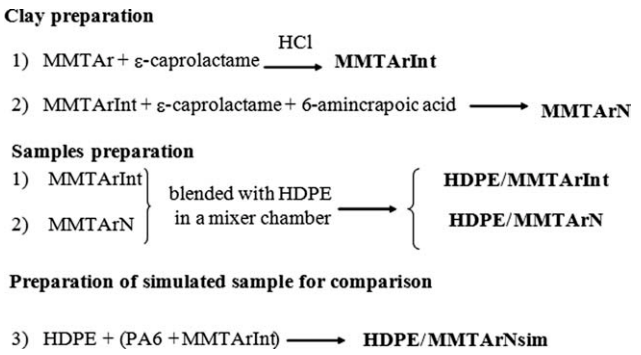

Figure 1 Scheme of samples preparation.

EXPERIMENTAL

Materials

PA6 (Nylodur) with [NH_2] = 55 meq/kg, M_w = 32,600 g/mol, T_m = 212–220°C and T_c = 173°C was provided by De Millus (Sao Paulo/Brazil). HDPE with a melt flow index (MFI) ASTM D 1238 0.41 g/10 min (190°C/5 kg), density (ASTM D792) 0.9530 g/cm^3 and softening point (ASTM D1525) 127°C was obtained from POLISUR (Buenos Aires/Argentina) (40055L), and ε-caprolactam from Braskem (Sao Paulo/Brazil).

An Argentinean montmorillonite (MMTAr) from Minarmco S.A. was used in this study.

Clay modification

Two modified clays were prepared:

1. Montmorillonite was intercalated with ε-caprolactam in acid medium, this specimen was named MMTArInt.
2. e-caprolactam and 6-aminocaproic acid used as accelerator were polymerized with the MMTArInt, yielding a PA6 homopolymer named MMTArN (clay/PA6), according to Kojima techniques.[12]

Preparation of HDPE/MMT composites

Figure 1 shows the schemes of procedures used to obtain nanocomposites by different methods.

The ability of PA6 in dispersing clays[11] was used to prepare the modified clay, and then it was mixed with HDPE. Mixing was performed in a mixer chamber equipped with roller rotors, Rheomix 600, Haake, at 240°C, 60 rpm during 10 min. Three composites were prepared starting from MMTArInt and MMTArN, one of them mixing MMTArInt with HDPE, the other, MMTArN with HDPE and finally, by melt intercalation techniques HDPE, PA6, and MMTArInt, labeled HDPE/MMTArNsim. The same percentage of PA6 and MMTArInt was used for both procedure, *in situ* polymerization and simulated polymerization (HDPE/MMTArNsim). Blend compositions are shown on Table I.

Film preparation

Films for characterization were manufactured by compression molding in a Carver press at 240°C. The films were cooled in a cold press at room temperature.

X-ray diffraction (XRD) and Infrared (IR) spectroscopy

Modified clays and blends were characterized using a Shimadzu DRX 6000 diffractometer with nickel filtered CuKα (λ = 1.54 Å) radiation operating at 40 kV and 30 mA. The data were recorded at 2θ rates of 2° per minute. Bragg's law (λ = 2d sin θ) was used to calculate the gallery spacing of the organoclay by the diffraction peak. Infrared spectra were obtained in a spectrometer FTIR 1720x, Perkin Elmer, at 2 cm^{-1} of resolution.

Scanning electron microscopy (SEM)

Characterization of blend morphology was performed in a SEM JEOL JSM-5600. Samples were immersed in liquid nitrogen and broken in two parts; the broken surface was analyzed by SEM after coating with gold.

Transmission electron microscopy (TEM)

TEM was carried out in Phillips CM-120 TEM equipment using an accelerator voltage of 120 kV. Ultrathin sections of the composites with a thickness of ~ 50 nm were prepared in the Ultracut RMC MT-7000 cryo-ultramicrotome equipped with a diamond knife Diatome CryoHisto 45° at −50°C. Samples were analyzed without any staining.

TABLE I
Composition of Polymer Blends

Sample	Organoclay w/w %	HDPE w/w %	PA6 w/w %	HDPE v/v %	PA6 v/v %
HDPE/MMTArInt	3	97	–	–	–
HDPE/MMTArN	3	40	57	44.88	53.42
HDPE/MMTArNsim	3	40	57	44.88	53.42

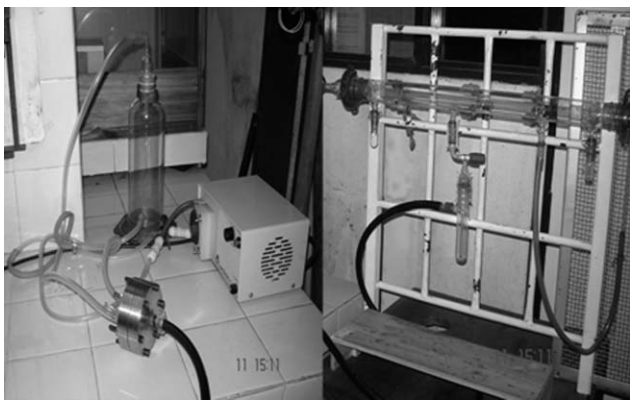

Figure 2 Standard apparatus for pervaporation.

Thermogravimetric analysis (TG)

TG was performed from room temperature to 700°C under N_2 flow (55 mL/min) at a heating rate of 10°C/min, with a thermal analyzer Rigaku model TAS 100. Samples were previously dehydrated at 90°C during 24 h.

Solubility

The samples were immersed in cyclohexane and thermostated at 50°C (323 K). The solubility values were calculated from the weight gain.

Pervaporation

The experiments were performed in standard pervaporation equipment (Fig. 2). Pervaporation test was carried out at constant temperature. Vacuum at the downstream side was maintained using a vacuum pump. Liquid nitrogen was used as cooler to collect all permeated vapors. A peristaltic pump was used to recirculate the solvent used (cyclohexane). A gravimetric method was used to measure the rate of pervaporation.

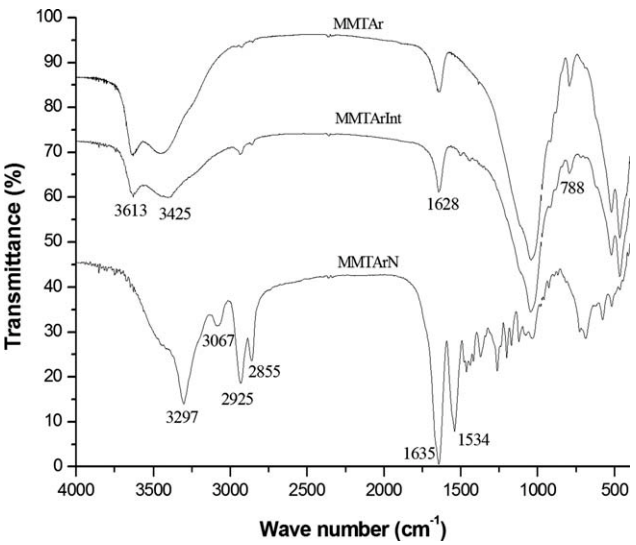

Figure 3 FTIR spectra of montmorillonite (MMTAr), intercalated montmorillonite (MMTArInt), and *in situ* polymerized montmorillonite (MMTArN).

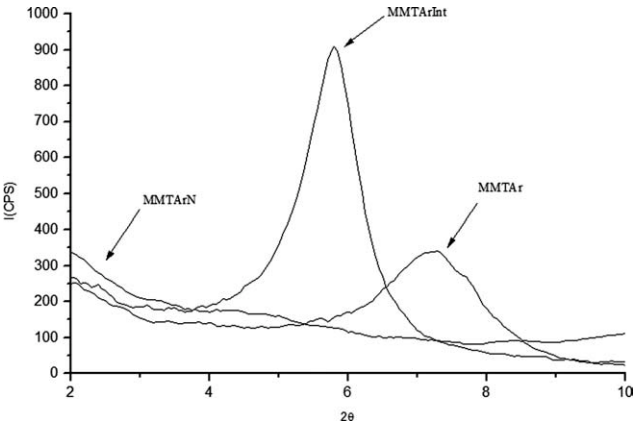

Figure 4 XRD patterns for natural and modified clays.

RESULTS AND DISCUSSION

The modified clays were characterized by IR spectroscopy and X-ray diffraction. Figure 3 shows the IR spectra and the characteristic absorption peaks of clay minerals. Three spectra are shown, the pristine montmorillonite, the intercalated montmorillonite (MMTArInt), and the *in situ* polymerized montmorillonite (MMTArN). As can be seen, characteristic natural clay peaks appear in all samples. Polyamide characteristic stretching bands, at 2855 cm^{-1} and 2925 cm^{-1}, confirm that a polymerization process occurred in MMTArN and the same bands, very weak, appear in MMTArInt spectrum.

The XRD results for the clays and their correspondent nanocomposites are presented graphically in Figures 4 and 5 and are also tabulated in Table II. Figure 4 shows XRD patterns for natural and

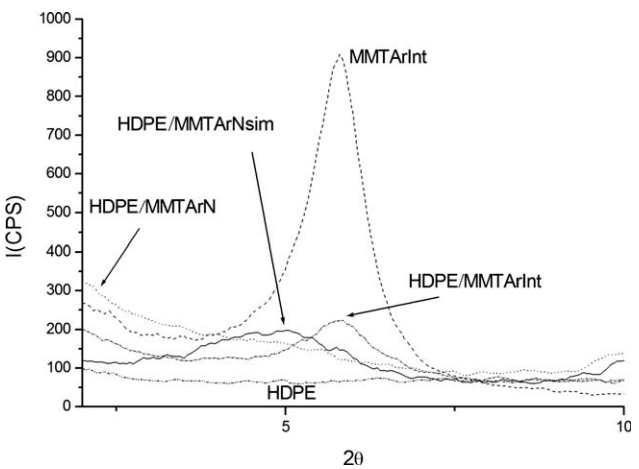

Figure 5 XRD patterns for polyethylene composites.

TABLE II
Interlayer of the Clays and Nanocomposites

Sample	2θ	Basal Spacing (Å)
MMTAr	7.4	12.1
MMTArInt	5.9	15.5
MMTArN	4.55	19.4
HDPE/MMTArInt	5.85	15.1
HDPE/MMTArN	3.10	28.5
HDPE/MMTArNsim	4.95	17.9

modified clays. The composites diffractograms are shown in Figure 5. The *d*-spacing of silicate layers in the organoclay were obtained from XRD patterns, Table II. The MMTAr basal spacing value (clay without treatment) was taken as reference. Table II shows that the MMTAr was intercalated with organic compound. The MMTAr peak in the MMTArInt shifted slightly to a lower angle, indicating that an intercalated structure with a *d*-spacing from 12.1 Å to 15.5 Å was obtained. The interlayer spacing in MMTArInt agrees with ε-aminocaproic acid dimension, and MMTArN shows the largest interlayer spacing (19.4 Å).

The XRD patterns of Figure 5 clearly shows that the exchange of MMTAr with ε-caprolactam and subsequent *in situ* polymerization shifted the (001) peak toward smaller angles ($2\theta = 4.55^\circ$), which correspond to a larger interlayer spacing ($d = 19.4$ Å) than that observed when the exchange is conducted with ε-caprolactam ($2\theta = 5.7^\circ$ and $d = 15.5$ Å). In the former case, the interlayer separation corresponds to chains of the PA6, whereas in the second case the separation corresponds to the thickness of the silicate layers and the diameter of the ε-aminocaproic acid molecule.

Both nanocomposites (HDPE/MMTArN and HDPE/MMTArNsim) were obtained and showed a mixed morphology of an intercalated and/or exfoliated structure. Nevertheless, the XRD curves showed an intercalation length of $d = 17.9$ Å for HDPE/MMTArNsim, and $d = 28.5$ Å for HDPE/MMTArN. According to the results, the preparation technique based on a combination of *in situ* polymerization and melt intercalation process (HDPE/MMTArN) was more effective, inducing a higher degree of exfoliation. These results are in accordance with our previous explanations and are supported by TEM data (Fig. 6).

As can be seen in Figure 5, exfoliation of HDPE/MMTArInt does not occur. In HDPE/MMTArN and HDPE/MMTArNsim composites mixed morphology of intercalated/exfoliated silicate layers seems to have taken place, resulting in structures in which the filler is dispersed in nanometer scale.

Different basal spaces were obtained from each polymer/clay composition. As it was said previously, the *d*-spacing of organoclay is higher than the clay without exchanging. The space was also increased even more with the presence of the PA 6, being the higher for the HDPE/MMTArN nanocomposites (28.5 Å).

To have a good and better insight on the MMTAr/ε-caprolactam system, it is necessary to consider the different interaction between the molecular species in the reaction medium.[13] For MMTArInt clay, used in both systems MMTArN and MMTArNsim, it is reasonable to assume that PA6 (from *in situ* polymerization) molecules form hydrogen bonds with the surface of silicate layers, and that they can also interact in the same way to form hydrogen bonds with OH from COOH end groups and [ ] groups of the silicate. Of course, interactions between silicate layers and PA6 molecules also can occur trough attached aminocaproic acid to silicate surface. The results obtained by Usuki et al.[10] suggested that the chain axes of ω-amino acids with a carbon number of eight or less were parallel to the silicate layers, and that the chain axis of those with the carbon number of 11 or more were slanted to the layers. A continuous phase appears comprised of PA 6 and the exfoliated clay. In this polar medium, HDPE forms nonpolar domains that do not interact with the continuous phase. SEM and TEM images clearly showed this process (Fig. 6).

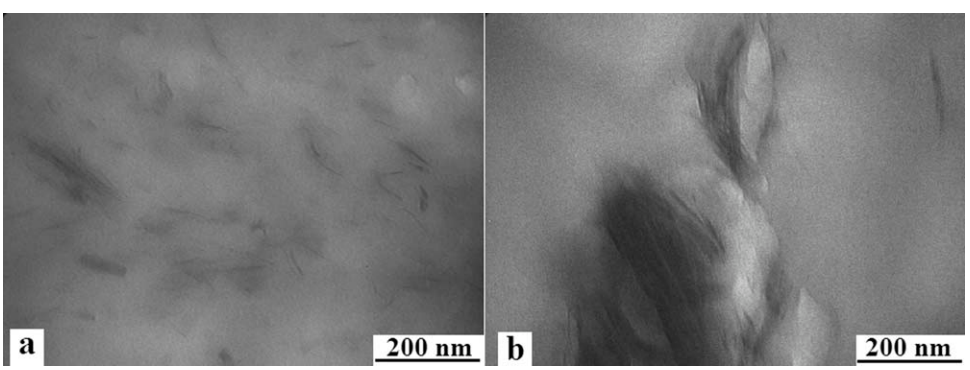

Figure 6 TEM images (a) HDPE/MMTARN and (b) HDPE/MMTARNsim.

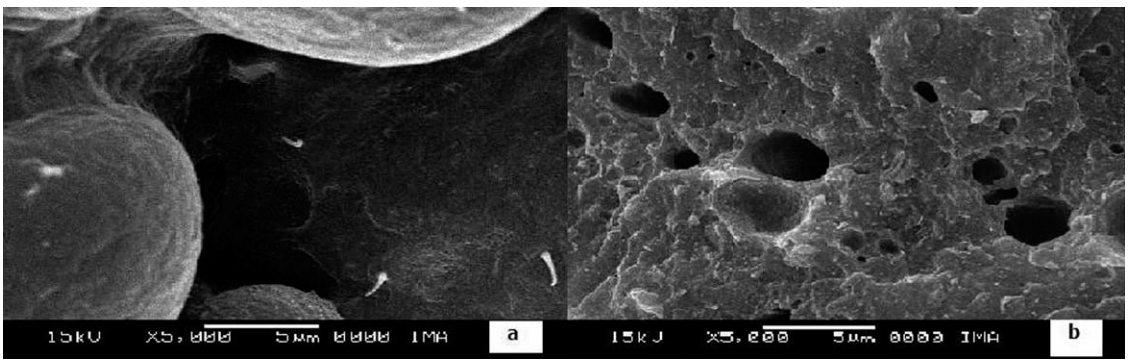

Figure 7 (a) SEM HDPE/MMTArNsim etched by formic acid vapor at room temperature and (b) SEM HDPE/MMTArNsim etched by toluene vapor.

To confirm that clay is dispersed in the nylon phase, the HDPE/MMTArNsim sample was etched in boiling toluene to remove HDPE component, and etched in formic acid at room temperature to remove PA 6 domains (Fig. 7).[13]

Figure 8 shows SEM images of HDPE/MMTArInt and PA6/MMTArInt blends. The latter compound was characterized and evaluated by Erdmann et al.[14] and it is introduced in this contribution for comparative purpose.

In Figure 8(a), it is shown that the MMTArInt is present in polyethylene phase as agglomerates, evidencing the absence of homogenization of both materials. In contrast, Figure 8(b) shows a completely homogeneous material because of the ability to disperse the nylon MMTArInt.

Comparing these figures with those in which the HDPE and PA6 were extracted, the presence of nonagglomerated is observed in both cases. If nylon phase had not exfoliated and/or intercalated the clay, clay agglomerates in the residual polyethylene where the polyamide phase was extracted should be observed [Fig. 7(a)]. This situation is observed in Figure 8(a), which shows that the MMTArInt was intercalated in the polyamide phase. The exfoliation and/or intercalation can not be observed by SEM, but was confirmed by TEM [Fig. 6(b)]. This figure corresponds to HDPE/PA6/MMTArInt sample, where there are two phases; the darker phase is attributed to the polyamide, where sheets of exfoliated clay were present.

Table III shows the data for the thermal degradation of HDPE composites and pure polymer materials. The data include the onset degradation temperature, the temperature at which 10% and 50% degradation occur, T0.1 and T0.5, respectively, the midpoint of the degradation, and the nonvolatile fraction at 500°C, denoted as residue. T 1° and T 2° represent the first and second temperature at the first and second maximum of weight loss.

Thermogravimetric curves of HDPE, PA6, and composites are reported in Figures 9 and 10. All thermal degradation profiles were obtained from TG and DTG curves. The curves profiles are apparently similar. However, the course of the decomposition seems to have been affected by the structure of the organoclay. Thermal degradation of HDPE and HDPE/PA6 takes place at temperatures higher than 443 and 406°C, respectively. There are no outstanding thermal degradation differences between HDPE and HDPE/MMTArInt, excepting the residual mass (Table III). Apparently, the HPDE degradation

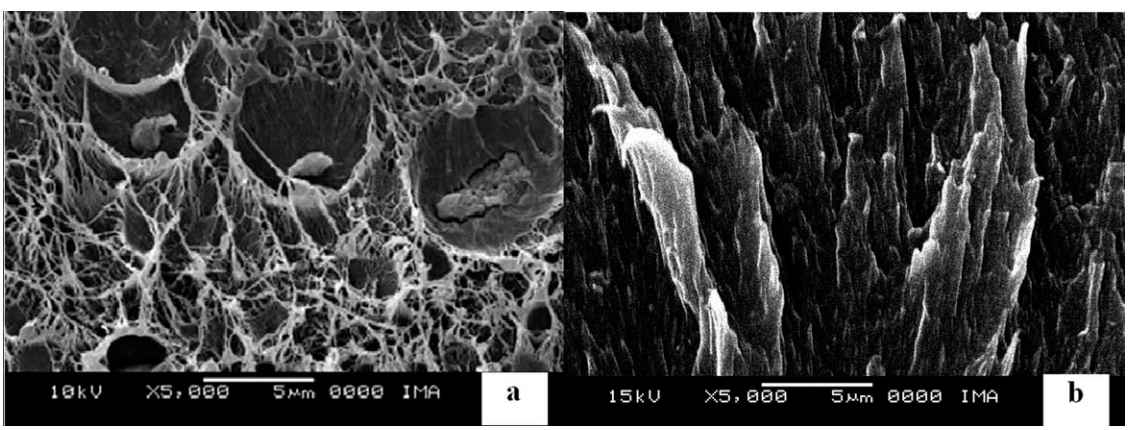

Figure 8 SEM of (a) HDPE/MMTArInt and (b) PA6/MMTArInt.

TABLE III
TGA Data, in Nitrogen, for HDPE Composites

Nanocomposites	T0.1 (°C)	T0.5 (°C)	Residue at 500°C (%)	T 1° max rate (°C)	T 2° max rate (°C)
PA6	402	446	0.0	90	456
HDPE	443	474	0.0	87	480
HDPE/MMTArInt	457	477	4.7	135	478
HDPE/MMTArN	397	451	5.6	114	455
HDPE/MMTArNsim	406	449	4.2	91	464
HDPE/PA6	419	458	0.0	82	464

temperatures and profiles were changed by the MMTArN and MMTArInt presences. The introduction of MMTArN in the HDPE and the introduction of MMTArInt in the HDPE/PA6 (HDPE/MMTArNsim) did not enhance the thermal stability of HDPE, as expected for exfoliated systems.

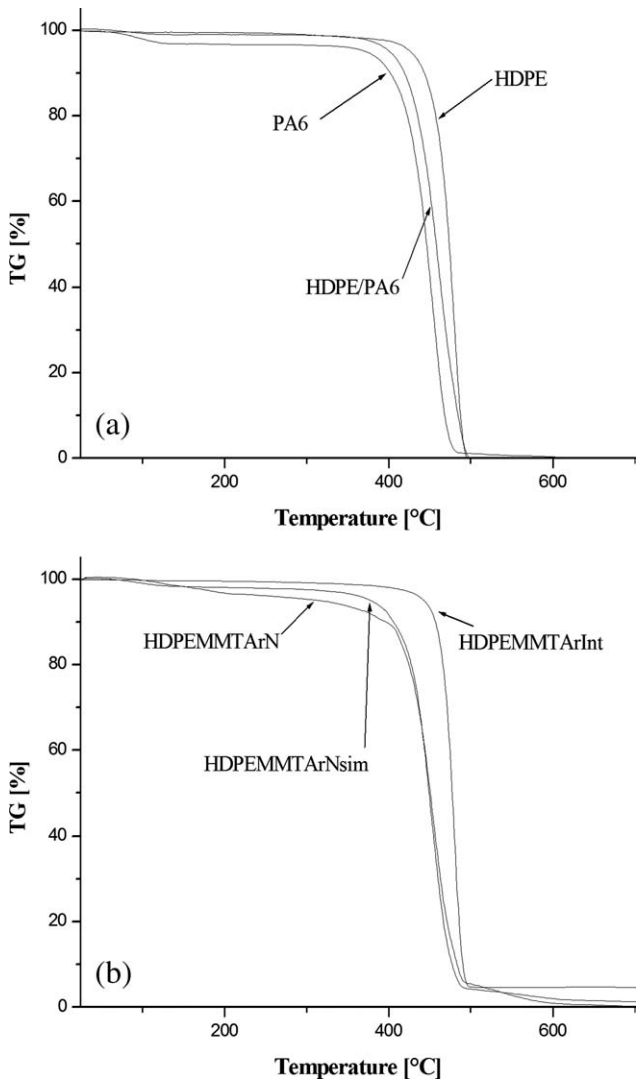

Figure 9 TG of HDPE, PA6, and HDPE/PA6 TG of HDPE/MMTArInt, HDPE/MMTArNsim, HDPE/MMTArN nanocomposites.

Comparison of degradation peak of DTG curves for different materials was also very informative. Figure 9 shows more clearly the influence of MMTArInt on HDPE/PA6 and MMTArN on HDPE thermal stability. A reduction in degradation temperatures with the addition of the MMTArN and MMTArNsim organoclays was observed. Whereas HDPE maximum rate of loss (%/°C) was presented at 480°C, the maximum of the HDPE/MMTArN and HDPE/MMTArsim curves were observed below 449°C (Fig. 10). The introduction of MMTArInt in HDPE did not produce effect in the temperatures.

It is important to note that, the obtained nanocomposites did not show any degradation at temperatures below 250°C, because of the degradation of low-molecular intercalated molecules as it is observed in nanocomposites containing tallow ammonium salts. It constitutes in an interesting advantage of these nanocomposites.

Preston et al.[15] have previously noted such effect of the MMTAr intercalated with hexadecyltrimethylammonium (HDTMA) on the onset of nonoxidative thermal degradation observed in others polymer nanocomposites. But, at nitrogen flow, polymer

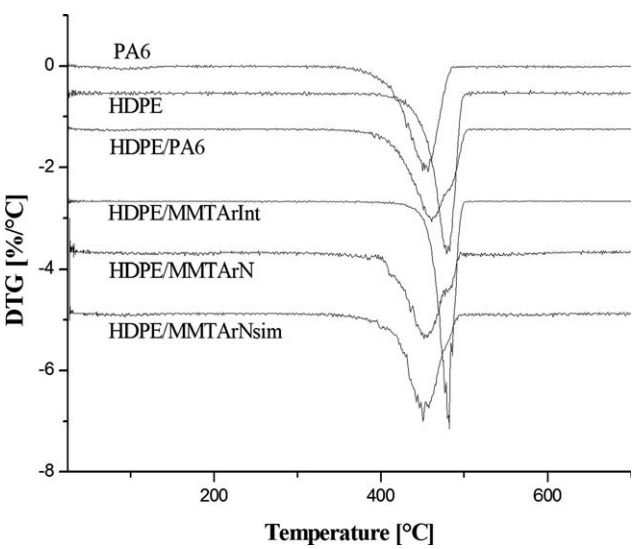

Figure 10 DTG of HDPE, HDPE/PA6, HDPE/MMTArInt, HDPE/MMTArNsim, HDPE/MMTArN nanocmposites.

thermal stability improvement is commonly expected when nanocomposites are obtained from organoclay addition, because of barrier effects.[15] An explanation for the behavior observed for the MMTArHDTMA-based nanocomposite may be possibly found considering the degradation mechanism. Davis et al.[16] have suggested that the PA6/organoclay decomposition may have resulted from a hydrolytic peptide scission. Clay and water are considered a special catalyst system in a polyamide 6 thermal degradation.[17,18] The barrier degradation retardant effect is also important, but in this case, the catalytic effect could be more significant.

Pervaporation and cyclohexane solubility

The barrier properties were determined by cyclohexane solubility and pervaporation. From these determinations, the activation energy (E_a) was calculated (Table IV). The activation energy for the films HDPE/MMTArInt, HDPE/MMTArN, and HDPE/MMTArNsim was practically the same, although the permeability of HDPE/MMTArN at 70°C (0.41 g mm/hm^2) was smaller than HDPE/MMTArNsim (1.85 g mm/hm^2) and smaller than HDPE/MMTArInt (13.95 g mm/hm^2). As mentioned the ability of polyamide 6 in dispersing clays has a positive effect on barrier properties of the HDPE. The activation energy for HDPE (13.0 Kcal/mol) was lower compared with PA 6 (17.3 Kcal/mol). The HDPE and PA 6 mixture has a high-permeability at 70°C, compared with pure components as shown in Table IV. This behavior is attributable to the materials inherent immiscibility that form the mixture, which would give rise to interfaces through which the diffusion of the solvent is facilitated.

The barrier properties were enhanced in the films with organoclay. Polymer/clay nanocomposites have highly ordered nanolayered structure that creates a tortuous path for cyclohexane whereas, conventional composites have a less restrictive path for cyclohexane in their microstructure.[10]

The nanocomposites have better barrier properties and solubility values, this is in accordance with what was expected, that is , the solvent has a higher difficulty to cross the nanocomposites than it has to cross a conventional composite bulk, as it is schematically shown in Figure 11. Between the two obtained nanocomposites, HDPE/MMTArNsim and HDPE/MMTArN, the last presents higher exfoliation degree and better barrier properties. This can be explained as the ability of PA 6 to disperse the organoclay is more effective by *in situ* polymerization than by melt intercalation process.

TABLE IV
Films Barrier Properties

Films	$S_{50°C}$ (% w/w)	$P_{70°C}$ (g mm/h m^2)	E_a (Kcal/mol)
HDPE	10.00	4.73	13.40
HDPE/MMTArInt	9.51	13.95	10.50
HDPE/MMTArN	1.16	0.41	10.53
HDPE/MMTArNsim	1.64	1.85	10.47
HDPE/PA6	2.29	30.01	7.03
PA6	1.52	9.13	17.31

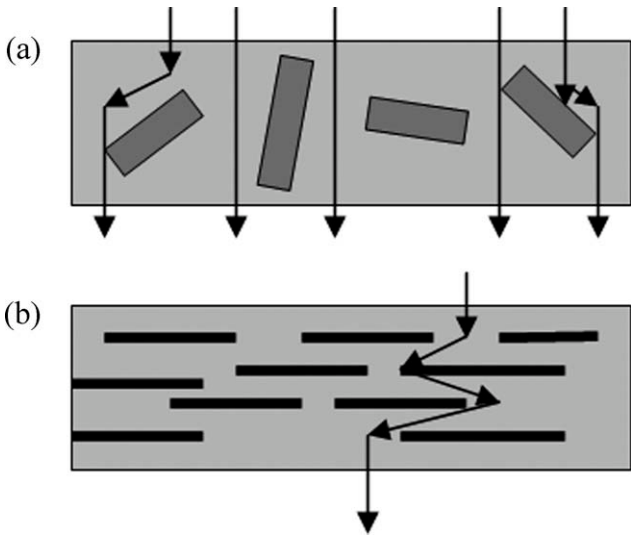

Figure 11 Tortuous diffusion path of conventional composites (a) and polymer/clay nanocomposites (b).

CONCLUSION

HDPE/PA6/organoclay nanocomposites were successfully prepared via melt compounding method and a combination *in situ* polymerization and melt intercalation process. This technique of nanocomposite preparation was more effective, inducing a higher degree of clay exfoliation, the clay being dispersed prevailing in the PA6 phase. The ability of PA6 in dispersing clays has a positive effect on the barrier properties of these HDPE-containing nanocomposites. The structure of the organoclay affects the course of thermal degradation process. DTG curves show a reduction in the composites degradation temperatures with the addition of MMTArN and MMTArNsim. No degradation was observed below 250°C, which is an interesting advantage of these nanocomposites. The activation energy of HDPE/PA6/organoclay nanocomposites show a change in the transport mechanism associated with the improvement in barrier properties. Adequate chemical modification of montmorillonite clay and preparation of polymer clay composite are necessary to generate HDPE/PA6/organoclay nanocomposites.

References

1. Alexandre, M.; Dubois, P. Mater Sci Eng 2000, 28, 1.
2. Yeh, J.; Jyan, C. Polym Eng Sci 1998, 38, 1482.
3. Gonzáles, I.; Eguiazábal, J. I. J Polym 2005, 46, 2978.
4. Ludueña, L.; Alvarez, V. A.; Vázques, A. Mater Sci Eng 2007, 460, 121.
5. Lepoittevin, B.; Pantoustier, N.; Devalckenaere, M.; Alexandre, M.; Calberg, C.; Jerome, R.; Henrist, C.; Rulmont, A.; Dubois, P. Polymer 2003, 44, 2033.
6. Lee, D.; Kim, H.; Yoon, K.; Min, K. E.; Seo, K. H.; Noh, S. K. Sci Technol Adv Mater 2005, 6, 457.
7. Dennis, H. R.; Hunter, D. L.; Chang, D.; Kim, S.; White, J. L.; Cho, J. W.; Paul, D. R. Polymer 2001, 42, 9513.
8. Yeh, J.; Fan-Chiang, C. J Appl Polym Sci 1997, 66, 2517.
9. Jiang, T.; Wang, Y.; Yeh, J.; Fan, Z.. Eur Polym J 2005, 41, 459.
10. Usuki, A.; Kojima, Y.; Kawasumi, M.; Okada, O.; Kurauchi, Y.; Kamigaito, O. J Mater Res 1993, 8, 1179.
11. Yoo, Y.; Park, C.; Lee, S. G.; Choi, K. Y.; Kim, D.; Lee, J. Macromol Chem Phys 2005, 206, 878.
12. Kojima, Y.; Usuki, A.; Kawasumi, A.; Okada, A.; Kurauchi, T.; Kamijaito, O. J Polym Sci Part A: Polym Chem 1993, 31, 983.
13. Erdmann, E.; Dias, M. L.; Pita, V. J. R. R.; Destéfanis, H.; Monasterio, F.; Acosta, D. Macromol Symp 2007, 258, 82.
14. Erdmann, E.; Dias, M. L.; Pita, V. J. R. R.; Monasterio, F.; Acosta, D.; Destéfanis, H. A. Mater Sci Forum 2008, 570, 78.
15. Preston, C. M. L.; Amarasinghe, G.; Hopwell, J. L.; Shanks, R. A.; Mathys, Z.. Polym Degrad Stab 2004, 84, 533.
16. Davis, R. D.; Gilman, J. W.; Vander Hart, D. L. Polym Degrad Stab 2003, 79, 111.
17. Bockhorn, H.; Donner, S.; Gernsbeck, M.; Hornung, A.; Hornung, U. J Anal Appl Pyrolysis 2001, 58, 79.